Hyperluminous starburst gives up its secrets

R. J. Ivison,[1,2] M. J. Page,[3] M. Cirasuolo,[1] C. M. Harrison,[1] V. Mainieri,[1] V. Arumugam[1,4] and U. Dudzevičiūtė[5]

[1] *European Southern Observatory, Karl-Schwarzschild-Strasse 2, D-85748 Garching, Germany*
[2] *Institute for Astronomy, University of Edinburgh, Blackford Hill, Edinburgh, EH9 3HJ*
[3] *Mullard Space Science Laboratory, University College London, Holmbury St. Mary, Dorking, Surrey RH5 6NT*
[4] *Institut de Radioastronomie Millimétrique, 300 rue de la Piscine, F-38406 Saint-Martin d'Hères, France*
[5] *Centre for Extragalactic Astronomy, Durham University, South Road, Durham DH1 3LE*

Submitted to MNRAS Main Journal, 2019 Xxxxxx; Manuscript ID: MN-19-XXXX-MJ

ABSTRACT

HATLAS J084933.4+021443 was identified as a dusty starburst via its rest-frame far-infrared (far-IR) emission. Multi-frequency imaging and spectroscopy revealed a cluster of four dusty galaxies at $z = 2.41$, covering 80 kpc. Here, we use ALMA to confirm a more distant, fifth protocluster member, and present X-ray and rest-frame optical imaging spectroscopy of the brightest, an unlensed hyperluminous IR galaxy (HyLIRG). The data reveal broad Hα and bright [N II] lines, and bright X-ray emission, characteristics that betray a Type-1 active galactic nucleus (AGN), strengthening evidence that AGN are ubiquitous amongst HyLIRGs. The accreting black hole is super massive, $M_{\rm bh} \approx 2\times10^9\,{\rm M}_\odot$, with little intrinsic absorption, $N_{\rm H} \approx 5\times10^{21}\,{\rm cm}^{-2}$. The X-ray properties suggest the accretion luminosity rivals that of the starburst, yet it is not obvious where this emerges in its panchromatic spectral energy distribution (SED). We outline three scenarios that could give rise to the observed characteristics, and how we might distinguish between them. In the first, we see the AGN through the host galaxy because of the cavity it excavates. In the others, the AGN is not co-spatial with the starburst, having been ejected via asymmetric gravitational radiation, or having evolved towards the naked quasar phase in an unseen companion.

Key words: galaxies: high-redshift — galaxies: active — galaxies: starburst — submillimetre: galaxies — infrared: galaxies

1 INTRODUCTION

Since the discovery of the first example amongst thousands of faint sources uncovered by the *Infrared Astronomical Satellite*, the origin of the prodigious energy that characterises hyperluminous infrared galaxies (HyLIRGs, defined such that $L_{\rm IR} \geq 10^{13}\,{\rm L}_\odot$) has been a topic of controversy — 'monsters or babies?' (Lutz & Tacconi 1999). Indeed, 'hidden quasar or protogalaxy?' was part of the title of the paper announcing the discovery of the now-famous $z = 2.3$ galaxy, IRAS FSC10214+4724 (Rowan-Robinson et al. 1991), which still qualifies as a HyLIRG even though it was eventually found to be strongly lensed (Graham & Liu 1995; Deane et al. 2013). A decade later, this same rare population made an appearance amongst early images obtained in the submm waveband, with the first submm-selected galaxy (SMG) being identified as a weakly lensed HyLIRG at $z = 2.8$, comprising a dust-obscured, gas-rich starburst alongside a broad-absorption-line (BAL) quasar (Ivison et al. 1998, 2010; Frayer et al. 1998, 2018; Vernet & Cimatti 2001).

As a result of the spatial resolution of the Atacama Large Millimetre Array (ALMA), many previously suspected HyLIRGs have been resolved into multiple, discrete ultraluminous IR galaxies (ULIRGs), some hovering around the HyLIRG threshold (e.g. Karim et al. 2013; Fu et al. 2013; Oteo et al. 2016, 2018; Riechers et al. 2017; Litke et al. 2019, cf. Younger et al. 2007, 2008; Riechers et al. 2013). Genuine, instrinsic HyLIRGs are thus known to be extraordinarily rare — indeed, to find the nearest examples one must search out to $z \approx 0.3$ (Rowan-Robinson & Wang 2010, cf. Efstathiou et al. 2014). Nevertheless, HyLIRGs are excellent laboratories with which to confront recent hydrodynamic simulations of isolated and merging galaxies (e.g. Hayward et al. 2011; Narayanan et al. 2015) which struggle to reproduce their number densities in the presence of the feedback required to match the local mass function. The luminosity of a HyLIRG implies a star-formation rate (SFR) of $\approx 3{,}400\,{\rm M}_\odot\,{\rm yr}^{-1}$; indeed, its SFR would remain substantial if the stellar initial mass function is top heavy (Zhang et al. 2018), or if there is a substantial contribution to $L_{\rm IR}$ from a powerful AGN as has often been suspected (e.g. Hines & Wills 1993; Franceschini et al. 2000). Either way, when observing HyLIRGs we are witnessing galaxy formation at its most extreme and it is important to understand which physical processes trigger these far-IR-luminous events, and the subsequent quenching mechanisms. Are these high-redshift starbursts similar to the ULIRGs seen locally, with the same efficiency in converting gas into stars, or do they have a higher star-formation efficiency? If the latter, why? Are the relations between metal content, star formation

and mass similar to other high-redshift galaxy populations? How do the starburst episodes relate to the growth of the central black holes?

As its name implies, HATLAS J084933.4+021443 (hereafter HATLAS J084933), was found in the largest extragalactic *Herschel* survey, *H*-ATLAS (Eales et al. 2010), with $S_{350\mu m}$ = 249 mJy (Valiante et al. 2016). Its redshift was determined quickly via multiple CO lines (z = 2.41 – Harris et al. 2012; Ivison et al. 2013; Gómez et al. 2018), suggesting $L_{\rm IR} \approx 6 \times 10^{13}\,{\rm L}_{\odot}$. Extensive panchromatic observations, including imaging at high spatial resolution with ALMA, the Jansky Very Large Array (JVLA), the Submillimetre Array and the Institut Radioastronomie Millimetrique's Plateau de Bure Interferometer (IRAM PdBI), revealed that HATLAS J084933 – like many other HyLIRGs (e.g. Karim et al. 2013) — breaks down into multiple gas-rich galaxies at the same redshift, covering ≈ 10 arcsec or ≈ 80 kpc in the plane of the sky, designated W, T, M and C (see[1] Figure 1 of Ivison et al. 2013 hereafter I13), each component a distinct ULIRG or HyLIRG. T is gravitationally amplified[2] by a foreground edge-on spiral; W is an unlensed HyLIRG. M and C are somewhat less luminous (still $L_{\rm IR} > 10^{12}\,{\rm L}_{\odot}$, so ULIRGs, and unlensed) yet gas-rich galaxies.

An unusually high intrinsic IR luminosity was first suspected for HATLAS J084933 because of its broad CO J = 1–0 line, ≈ 1,180 km s^{-1} FWHM, as detected by the Greenbank Telescope (GBT), which Harris et al. (2012) argued was consistent with no gravitational amplification. However, although W does have an unusually broad CO line, 825 ± 115 km s^{-1} FWHM, and is unlensed, the overall line width was shown by I13 to owe much to the velocity dispersion of the aforementioned group of luminous starbursts found within the GBT beam.

High-resolution (∼ 0.3-arcsec) 3-D spectroscopy obtained with JVLA and the IRAM PdBI in ^{12}CO J = 1–0 and 4–3, respectively, traced the molecular gas dynamics on scales of ≈ 1 kpc, measuring the spatial extent of the gas (∼ 1 arcsec, or ∼ 8 kpc), its mass (and density), Toomre parameter and the mid-plane hydrostatic ISM pressure. Later ALMA observations suggested that the far-IR emission of the most luminous component, W, corresponds to greybody emission from dust at a single temperature, ≈ 40 K, throughout the full extent of the galaxy (Gómez et al. 2018).

In all of these long-wavelength studies, and also with regard to its rest-frame optical–through–radio SED, HATLAS J084933-W resembles a starburst, with no obvious sign of any influence from an AGN, though — like mergers and interactions — accreting black holes are often difficult to identify in dusty starbursts with anything but the deepest and most complete of datasets. In this paper we present new observations of HATLAS J084933 obtained using the Atacama Large Millimetre/Submillimetre Array (ALMA), the European Space Agency's *XMM-Newton* space observatory and the KMOS spectrograph on UT1 of the European Southern Observatory's Very Large Telescope, to further elucidate the nature of this galaxy: hidden quasar, or protogalaxy? Monster, or baby?

The paper is organised as follows: § 2 describes the observations and data reduction. § 3 presents the results, with our discussion of those results in § 4. We summarise our results and draw conclusions in § 5. Throughout, we adopt a standard Λ-CDM cosmology with $\Omega_{\rm m}$ = 0.3, Ω_{Λ} = 0.7 and H_0 = 70 km s^{-1} Mpc^{-1}, such that 1 arcsec corresponds to 8.1 kpc at z = 2.41.

[1] Alternatively, the layout of these galaxies is shown later in this paper.
[2] Weakly — by less than a factor two; intrinsically, T is still a HyLIRG.

2 OBSERVATIONS AND DATA REDUCTION

2.1 KMOS/VLT

The KMOS observations were carried out during ESO observing period P94, under the observing programme 094.A – 0214(A). We adopted the standard object-sky-object nod-to-sky observation pattern, with 300-s exposures and an alternating 0.2- and 0.1-arcsec dither pattern to improve the spatial sampling. The target was observed in the K band, with a total integration time (on source) of 80 min, with a median seeing of 0.7 arcsec.

The data reduction was performed by using SPARK (Software Package for Astronomical Reduction with KMOS – Davies et al. 2013), implemented using ESOREX (ESO Recipe Execution Tool – Freudling et al. 2013). Each of the 300-s exposures was reconstructed independently, wavelength calibrated and sky subtracted using the closest sky exposure, and finally re-sampled into a data cube with 0.1×0.1 arcsec^2 spaxels. In order to improve the sky subtraction we used the SKYTWEAK option within SPARK (Davies 2007), which accounts for the time variability of the various OH sky-line families. Standard-star observations were carried out on the same night as the science observations and used for telluric correction and flux calibration. The individual 300-s cubes were finally combined together to create a stacked cube.

2.2 XMM-Newton

HATLAS J084933 was observed with *XMM-Newton* on 2017 April 22–23 (AO15, proposal 078435). The resulting data from the European Photon Imaging Camera (EPIC), which comprises three X-ray charge-coupled device cameras operated in a so-called 'photon-counting mode', were reduced with version 15.0 of the *XMM-Newton* Science Analysis Software (SAS). The *XMM-Newton* observation was significantly affected by particle background flaring events, from which the data were screened on the basis of the full-field count rate above 5 keV. After filtering out the high-background periods, the net exposure times were 27, 26 and 26 ks in the MOS 1 and MOS 2 cameras and the pn camera, respectively.

Images were constructed in four bands: 0.2–0.5, 0.5–2, 2–5 and 5-10 keV. Background images were constructed following the procedure described by Loaring et al. (2005). The images were searched simultaneously for sources in the four energy bands using the standard SAS tasks, EBOXDETECT and EMLDETECT. The astrometric solution of the images was refined by cross-correlating the X-ray source list with optical sources from the Sloan Digital Sky Survey (SDSS – Adelman-McCarthy et al. 2008) using the SAS task, EPOSCORR.

A point-like X-ray source was found at α = 08h 49m 33.59s, δ = +02° 14′ 44.″6 (J2000) with a 1-σ statistical uncertainty of 0.4 arcsec, which includes the contribution from the astrometric cross match to SDSS. This position is coincident with that of the unlensed[3] component, W, of HATLAS J084933. We have verified by examination of the 3XMM catalogue (Rosen et al. 2016) that our 0.4-arcsec positional uncertainty is reasonable for an on-axis source with comparable signal-to-noise ratio. Note that the point spread function (PSF) of EPIC, at around 6 arcsec full-width half maximum (FWHM), is sufficiently large that minor contributions to

[3] An optical point source visible immediately to the west of W is a star. As described by I13, it is unable to provide any significant gravitational amplification; the X-ray data reported here are not compatible with stellar emission, thus we can reliably associate the X-ray emission with W.

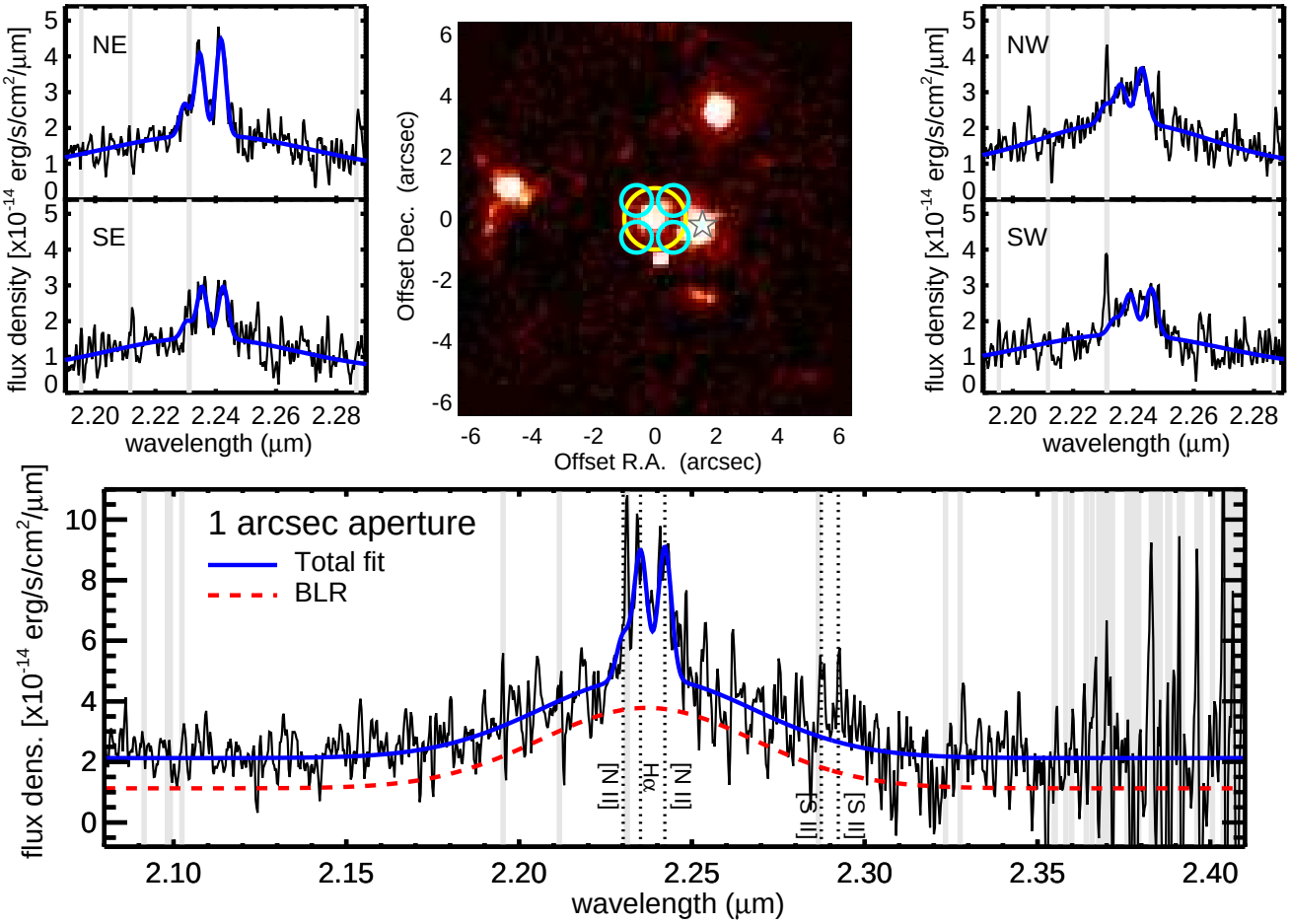

Figure 1. Extracted inside a 1-arcsec-diameter aperture (yellow circle, overlaid on the *Hubble Space Telescope (HST)* F110W image from I13), the lower panel shows the broad Hα emission, spanning 9,700 km s^{-1} FWHM, in component W of HATLAS J084933 as observed by VLT/KMOS, unambiguously revealing the presence of a previously unseen broad-line AGN. [N II] at 654.986, 658.527 nm and [S II] can also be seen (and is also marked). The other four spectra illustrate the variation in the ratio of [N II] to Hα, which increases markedly to the North-East (NE), as sampled by small off-centre apertures (the four blue circles). It is unfortunate that the blue [N II] line falls almost exactly on a sky line (this region was masked during the fitting); however, this issue is mitigated by the fact that this blue [N II] line has a fixed wavelength offset and flux ratio ($3.06^{-1}\times$) with respect to the redder (brighter) component of the [N II] doublet. Given the bright red component, we can be confident that the blue component is buried under the sky line. N is up; E is to the left; offsets from α_{2000} = 132°.3900 and δ_{2000} = 2°.2457 are marked in arcsec. A known star is labelled.

the X-ray flux from the other components of the HATLAS J084933 system may be hidden in the wings of the PSF. Nevertheless, the precise positional coincidence of the X-ray source with component W implies that the X-ray emission is dominated by this component.

We extracted X-ray spectra in the three EPIC cameras from a circular region of 15 arcsec radius, centred on the X-ray source. Background spectra were obtained from an annular region surrounding the source, from which detected X-ray sources were excised. Event patterns 0–12 were included in the spectra derived from MOS, while for the spectra derived from the pn camera we used patterns 0–4 above 0.4 keV and only pattern 0 between 0.2 and 0.4 keV. For MOS, channels corresponding to the strong 1.5-keV Al Kα background emission line (Lumb et al. 2002) were excluded. The spectra of the target from the different EPIC cameras were then combined to form a single spectrum, and the corresponding response matrices and background spectra were combined in an appropriate fashion to form a single response matrix and a single background spectrum, following the method described in Appendix A of Page et al. (2003). Finally, the spectrum was grouped to a minimum of 20 counts per bin.

2.3 ALMA

The ALMA band-6 245-GHz (1.22-mm) data used here were obtained for project 2013.1.00164.S, targeting the CH^+ line (Falgarone et al. 2017). Our resulting continuum image, where we have discarded the channels around the CH^+ line, was made using the CLEAN task in the Common Astronomy Software Application package (CASA – McMullin et al. 2007). The image has an r.m.s. noise level, σ = 38 μJy beam^{-1}, and the synthesised beam measures 0.49 × 0.48 arcsec^2 FWHM, with the major axis at a position angle, measured East of North, of 127°.

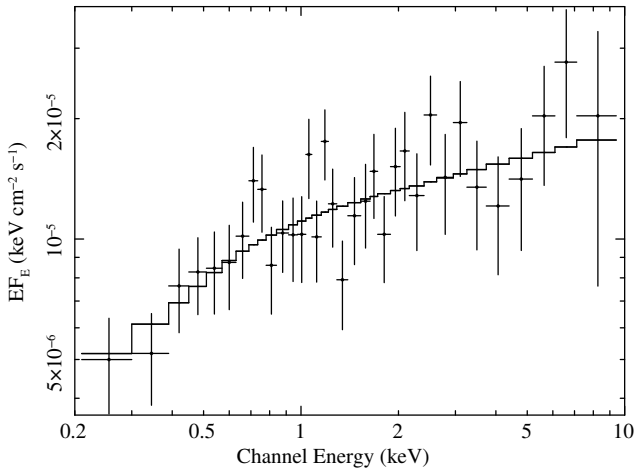

Figure 2. The *XMM-Newton* EPIC X-ray spectrum of HATLAS J084933. The data points correspond to the measured spectrum and the stepped line corresponds to the best-fitting absorbed power-law model. Both model and data have been divided by the product of the effective area and Galactic column as a function of energy and are plotted as EF_E, channel energy multipled by the energy flux per unit energy, so that an unabsorbed power law with $\alpha = +1$ would correspond to a horizontal line.

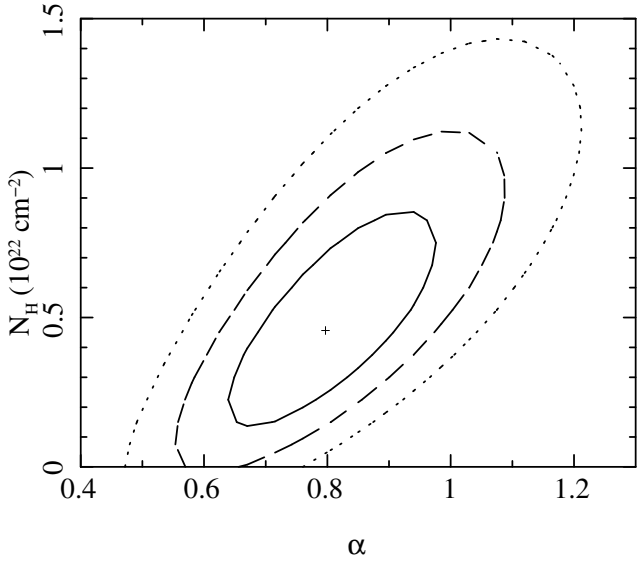

Figure 3. Confidence contours for power-law slope, α, and intrinsic column density, N_H, from the model fit to the *XMM-Newton* EPIC X-ray spectrum. The solid, dashed and dotted contours correspond to $\Delta\chi^2$ of 2.3, 6.2 and 11.8 respectively, equivalent to 68, 95 and 99.7 per cent confidence regions for two interesting parameters. The best-fit model parameters are indicated with a small cross.

3 RESULTS

Here, we outline what can be deduced from the new rest-frame optical spectroscopy, X-ray spectroscopy, and the submm imaging, as described in the previous section.

Fig. 1 presents our new KMOS spectrum of component W of HATLAS J084933, extracted in a 1-arcsec-diameter aperture. The Balmer Hα 656.461-nm emission is very strong indeed, and broad, where in SMGs it is normally a combination of weak and narrow lines offset spatially from broader (few $\times 1000\,\mathrm{km\,s^{-1}}$) compact components (Menéndez-Delmestre et al. 2013). We fit Gaussians simultaneously to the broad and narrow Hα components, and to the [N II] doublet at 654.986 and 658.527 nm with a red/blue [N II] line ratio of 3.06, with all the narrow lines tied to the same redshift and line width[4], and we also fit simultaneously to the continuum. The strongest sky lines (marked in grey in Fig. 1) were masked during the fitting process. We find that the broad [narrow] Hα lines span 9,700 [600] km s^{-1} FWHM, with the narrow lines[5] at $z_{\rm lsr} = 2.4048$. The line fluxes determined for the narrow and broad Hα lines, accurate to $\approx$ 10 per cent, are 2.0×10^{-17} and 2.0×10^{-16} ergs s^{-1} cm^{-2}. The flux and width of the broad line imply a black hole mass, $M_{\rm bh} \approx 2 \times 10^9\,\mathrm{M_\odot}$ (Schulze et al. 2018), i.e. a super-massive black hole (SMBH).

There can be no doubt, therefore, based on the characteristics of the Hα emission line profile, that a broad-line Type-1 AGN is present in the HATLAS J084933-W system.

In passing we note that the ratio of [N II] to Hα increases markedly to the NE of the combined continuum/line centroid, as illustrated in Fig. 1, suggestive of an ionisation cone.

We turn now to the data from *XMM/Newton*. The X-ray spectrum was modelled using version 11.3 of the X-ray spectral fitting package, XSPEC. An absorbed power-law model was fitted to the spectrum, in which the absorption was the product of cold Galactic photoelectric absorption with a fixed column density of $N_{\rm H} = 2.9 \times 10^{20}\,\mathrm{cm^{-2}}$, and cold photoelectric absorption at $z = 2.41$, corresponding to the rest frame of HATLAS J084933, for which the column density was a free parameter in the fit. The spectrum and best-fitting model are shown in Fig. 2. The fit yielded a χ^2 of 22.3 for 31 degrees of freedom, implying that the model fits the data well. Fig. 3 shows the confidence contours for the intrinsic ($z = 2.41$) column density, $N_{\rm H}$, and power-law energy index, α, defined such that $S_\nu \propto \nu^{-\alpha}$. The best-fitting power-law index, $\alpha = 0.8 \pm 0.1$, typical for QSOs at $z \approx$ 2–3 (e.g. Mateos et al. 2005, 2010). The best-fitting intrinsic column density, $N_{\rm H} = (5 \pm 3) \times 10^{21}\,\mathrm{cm^{-2}}$. Zero intrinsic column density corresponds to a $\Delta\chi^2$ of 5.9, so the intrinsic absorption is only marginally significant (2σ). The 3σ upper limit to the intrinsic column is $1.2 \times 10^{22}\,\mathrm{cm^{-2}}$. The best-fitting model implies a 2–10-keV flux of $4.1 \times 10^{-14}\,\mathrm{erg\,cm^{-2}\,s^{-1}}$ and a 2–10-keV luminosity, $L_{\rm X} = 1.4 \times 10^{45}\,\mathrm{erg\,s^{-1}}$, once corrected for Galactic and intrinsic absorption.

This X-ray luminosity is orders of magnitude brighter[6] than we would expect for X-ray emission due to star formation ($L_{\rm X} \lesssim 0.004\,L_{\rm IR}$ – Alexander et al. 2005a) and brighter than any of the 21 X-ray-luminous SMGs found by Stach et al. (2019) amongst the 274 SMGs covered by the $\geq$ 200-ks *Chandra* X-UDS (Kocevski et al. 2018) observations. We find $L_{\rm X} \sim 0.011\,L_{\rm IR}$, roughly consistent with both the 'AGN-classified SMGs' of Alexander et al. (2005b) and the quasars catalogued by Elvis et al. (1994), with both $L_{\rm X}$ and $L_{\rm IR}$ similar to IRAS F15307+3252, a hyperluminous Seyfert 2 quasar at $z = 0.93$ about which relatively little is known (Cutri et al. 1994; Ruiz et al. 2007).

[4] [S II] can also be seen, weakly; this wavelength range was excluded from the fits.

[5] Recall that the three CO lines observed towards HATLAS J084933-W have an error-weighted average redshift, $z_{\rm lsr} = 2.4068 \pm 0.0002$, so offset away from us along the line of sight from the rest-frame optical lines by $\approx 600\,\mathrm{km\,s^{-1}}$.

[6] We must acknowledge, of course, that we cannot yet know whether the X-ray emission is variable.

Our X-ray data thus corroborate the conclusion of our rest-frame optical spectroscopy: HATLAS J084933-W hosts an AGN.

To estimate the *bolometric* luminosity of the AGN, we begin by translating the K-corrected X-ray luminosity to an expected rest-frame ultraviolet (UV) 250-nm luminosity via the logarithmic slope, $\alpha_{\rm OX}$, which connects the 250-nm and 2-keV points on the SED. Using equation 4 from Just et al. (2007), we obtain[7] $\alpha_{\rm OX} = 1.63$. Taking the resulting UV luminosity, we use the bolometric correction from figure 12 of Richards et al. (2006) to arrive at an overall bolometric correction factor of 110× the 2–10-keV luminosity, implying a bolometric luminosity of 1.6×10^{47} erg s^{-1}, or $\log L_{\rm bol}/{\rm L}_\odot \approx 13.62$, so of the same order as the IR luminosity of the starburst, $\log L_{\rm IR}/{\rm L}_\odot = 13.52 \pm 0.04$ (I13).

To assess the uncertainty in our estimate of the AGN's bolometric luminosity, we combine in quadrature the r.m.s. scatter in $\alpha_{\rm OX}$ from Strateva et al. (2005) and in the UV-to-bolometric correction factor from Richards et al. (2006), obtaining an overall 1σ logarithmic uncertainty of 0.31, so roughly a factor of two.

In the absence of a measurement of the Balmer decrement, we can make a crude estimate of the optical extinction towards the AGN using the well-documented correlation between the logarithms of Hα and X-ray luminosity. For this, we use the regression of the full sample of Panessa et al. (2006), given by the fourth row of their table 3 and shown in the right-hand panel of their figure 4, adjusting for the different value of H_0 that they adopted. For our observed 2–10-keV luminosity, we would expect an intrinsic Hα luminosity of 4.7×10^{43} erg s^{-1}, where the measured flux of the broad Hα component corresponds to a luminosity of 9×10^{42} erg s^{-1}. To reconcile these predicted and observed luminosities requires 1.8 magnitudes of extinction. Taking the scatter of the Panessa et al. (2006) sample about the regression into account, together with the measurement errors on the Hα and X-ray luminosities, we estimate a 1σ uncertainty of 1.3 magnitudes on the implied extinction. Translating to A_V from the extinction experienced at the wavelength of Hα using the $R_V = 3.1$ extinction law of Cardelli et al. (1989) gives $A_V = 2.2 \pm 1.6$. Güver & Özel (2009) suggest that $N_{\rm H} = (2.21 \pm 0.09) \times 10^{21} A_V$ for a Milky-Way-like dust-to-gas ratio, so we find $N_{\rm H} = (4.8 \pm 3.5) \times 10^{21}$ cm^{-2}, perfectly consistent with the column density we determined using our X-ray measurements.

Any intrinsic absorption towards the AGN is thus likely to be rather small, which is perhaps surprising for a galaxy that contains such immense quantities of molecular gas, and with $\approx 2 \times 10^9$ M$_\odot$ of dust that we have already noted is well fit with greybody emission at a single temperature over the full extent of the galaxy (Gómez et al. 2018), bearing in mind that typical SMGs are thought to be optically thick out to $\approx 75\,\mu$m, with $N_{\rm H} \approx 10^{24}$ cm^{-2} and $A_V \approx 500$ (Simpson et al. 2017).

Moving now to the ALMA data, Fig. 4 presents our ALMA band-6 continuum image of HATLAS J084933 with contours superimposed on the *HST* F110W image from I13. In a separate panel of Fig. 4 we show the JVLA ^{12}CO $J = 1$–0 imaging and the *Spitzer* IRAC imaging from I13. We do this to illustrate that a band-6 continuum source, detected at 6σ, which we denote component 'E', which lies ≈ 12 arcsec to the north of component T, can now be seen to be coincident with a very red galaxy that was detected by IRAC, as well as being detected in CO, also at 6σ, but which is not seen in the F110W *HST* image. E lies in a confused region of the

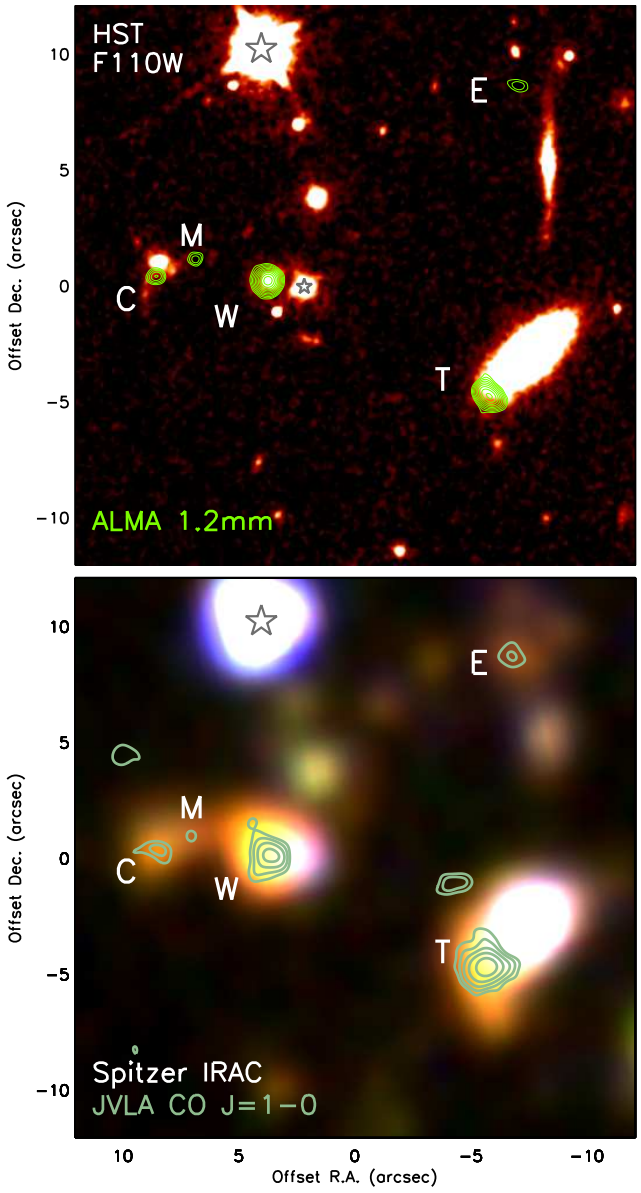

Figure 4. *Top:* band-6 245-GHz (1.22-mm) continuum emission superimposed as contours on the *HST* F110W imaging of HATLAS J084933. *Bottom:* contours of ^{12}CO $J = 1$–0 emission, collapsed optimally for each object, superimposed on a three-colour image comprising a heavily smoothed $J + H + K_{\rm s}$ image from VISTA as the blue channel plus the *Spitzer* IRAC 3.6- and 4.5-μm data, all from I13. The object marked 'E', north of T, can now be considered robustly identified — via the positional coincidence of faint 1.2-mm and CO emission with a red IRAC counterpart — as a fifth dusty, gas-rich galaxy in this $z = 2.4$ proto-cluster. Contours are plotted at $-3, 3 \times \sigma$, with $\sqrt{2}$-spaced increments thereafter, where σ is the local noise level. N is up; E is to the left; offsets from $\alpha_{2000} = 132^\circ.3889$ and $\delta_{2000} = 2^\circ.2457$ are marked in arcsec. Known stars are labelled.

maps obtained by the *Wide-field Infrared Survey Explorer* (*WISE* – Wright et al. 2010) and a limit cannot be set that is both meaningful and useful. Component E can thus be added to the inventory of dusty, gas-rich galaxies that form part of the protocluster associated with HATLAS J084933, making five in total, covering ≈ 15 arcsec or ≈ 120 kpc.

As seen in the CO $J = 1$–0 image, integrated over its full line width, E subtends ≈ 7.3 kpc. Consistent measurements of $I_{\rm CO}$

[7] Note that the minus sign is explicit in our definition of $\alpha_{\rm OX}$ but not in that used by Just et al. (2007).

Table 1. Basic observational properties of component E

Wavelength	S_ν	Comment
1.1 μm	$3\sigma < 0.8$	μJy; F110W
2.15 μm	$3\sigma < 9.1$	μJy; VISTA K_S
3.6 μm	7.9 ± 1.0	μJy; IRAC
4.5 μm	10.3 ± 1.5	μJy; IRAC
1.22 mm[a]	1.47 ± 0.24	mJy; ALMA
5.9 cm	$3\sigma < 45$	μJy; JVLA
R.A.	08:49:32.867 (±0.003)	J2000
Dec.	+02:14:53.12 (±0.03)	J2000
log $L_{\rm IR}$[b]	$12.8^{+0.1}_{-0.2}$	$L_\odot$
SFR	650	$M_\odot$ yr^{-1} (see text)
FWHM CO $J=1-0$	7.3 ± 1.8	kpc
CO $J=1-0$ $I_{\rm CO}$	0.27 ± 0.06	Jy km s^{-1}
CO $J=1-0$ FWHM	1380 ± 410	km s^{-1}
CO $J=1-0$ $z_{\rm LSR}$	2.4151 ± 0.0018	
CO $J=1-0$ $L'_{\rm CO}$	76 ± 17	10^9 K km s^{-1} pc^2
CO $J=1-0$ $L_{\rm CO}$	3.9 ± 0.9	10^6 $L_\odot$
log $M^{\rm c}_{\rm H_2+He}$	10.8 ± 0.2	$M_\odot$
log $M_{\rm stars}$	10.3 ± 0.2	$M_\odot$
SFE	120	$L_\odot$ $M_\odot^{-1}$

[a]Peak 1.22-mm flux density, 660 ± 75 μJy beam^{-1}, so resolved by the 0.49×0.48 arcsec^2 FWHM beam.
[b]Scaled from component W, where $S_{1.22{\rm mm}} = 8.29 \pm 0.13$ mJy and log $L_{\rm IR} = 13.52$, thereby adopting the same SED as W for component E.
[c]For $\alpha_{\rm CO} = 0.8\,M_\odot$ (K km s^{-1} pc^2)$^{-1}$.

were obtained from this image and from a Gaussian fit to the spectrum extracted at the peak and corrected for $I_{\rm total}/I_{\rm peak}$. E lies close to the redshifts of M and C, somewhat redward of W and T, and thus further helps to explain the broad line seen originally by the $\approx$ 22-arcsec primary beam of GBT (Harris et al. 2012). The line is considerably broader than those of the other cluster galaxies, $\approx 1{,}380$ km s^{-1} FWHM, albeit with a large uncertainty. The signal to noise is too low for us to be fully confident, but two gas clumps may be involved, distinct both spatially and in redshift, or there could be a rotating gas disk, as with W and T, this time along PA $\approx 45°$, with the reddest component to the north east. Scaling from the band-6 flux density and SED of component W, component E has an IR luminosity of approximately 6×10^{12} $L_\odot$. Following Kennicutt (1998), this implies an SFR of 650 $M_\odot$ yr^{-1} for a Chabrier (2003) stellar initial mass function (IMF), or considerably less for the IMF observed in distant, dusty starbursts by Zhang et al. (2018). E contains approximately 6×10^{10} and 2×10^{10} $M_\odot$ of gas and stars, respectively. Its basic observational properties are listed in Table 1.

Component E is not detected in our *XMM-Newton* images, and is in the wings of the PSF of component W. We measured the counts in a 10-arcsec-radius aperture at the position of component E and can set a 3σ 2–10-keV upper limit of 8.5×10^{-15} erg cm^{-2} s^{-1}.

4 DISCUSSION

Before discussing plausible explanations for the properties of HATLAS J084933-W, let us first look at our results in the context of other relevant samples. The X-ray properties of HATLAS J084933-W are consistent with those of the majority of the 14 HyLIRGs at $z = 0.3$–2.0 observed in X-rays by Ruiz et al. (2007), where the sample was selected to contain a range of examples of the HyLIRG population, including Type 1 and 2 QSOs, so significantly biased towards those containing AGN. Compared to the Lusso et al. (2012) sample of 929 AGN, selected over a $\approx$ 2-deg^2 field via X-rays, only five have higher bolometric luminosities than HATLAS J084933-W; its redshift is amongst the most distant decile of Type-1 AGN; its absorbing column is roughly 7× the average $N_{\rm H}$ for an X-ray-selected Type-1 AGN — not particularly unusual — and half the average for a Type-2 AGN.

We know that there are no clear signatures of an AGN in the rest-frame UV spectrum of HATLAS J084933-W, where the Keck spectroscopy of I13 revealed only faint C II] at rest-frame 232.6 nm, consistent with considerable dust obscuration. Is there any other indication from existing observations of HATLAS J084933-W that it might harbour a powerful AGN? Is the panchromatic SED of HATLAS J084933-W more consistent with a typical SMG, or with a luminous AGN?

The SED of HATLAS J084933-W was not presented blueward of $\lambda_{\rm obs} = 880$ nm by I13, but it has since been observed as part of the wide layer of the Hyper Suprime-Cam Subaru Strategic Program (Aihara et al. 2018), with $g = 23.69 \pm 0.26$, $r = 22.59 \pm 0.18$, $i = 21.92 \pm 0.13$, $z = 21.41 \pm 0.09$ and $y = 21.08 \pm 0.08$ AB mag. We also note that *WISE* obtained a 3σ detection consistent with the position of component W of HATLAS J084933 - albeit with poor spatial resolution, 6.5 arcsec FWHM — in its W3 band at 12 μm, with a flux density of 420 ± 140 μJy. An even more tentative ($< 3\sigma$) detection was made in the W4 band (12 arcsec FWHM) at 22 μm: 3.3 ± 1.3 mJy. These data represent weak evidence that the mid-IR SED tends towards the AGN region of colour-colour space outlined in diagnostic plots (e.g. Ivison et al. 2004; Lacy et al. 2004).

An updated SED for HATLAS J084933-W, now spanning rest-frame UV–radio wavelengths, is shown in Fig. 5. For comparison, Fig. 5 also shows the median SED of over 700 ALMA-identified SMGs from U. Dudzevičiūtė et al. (in prep), and the well-sampled SEDs of the dust-rich, Type-1 AGNs, APM 08279+5255 and BR 1202−0725 (Irwin et al. 1998; McMahon et al. 1994; Leipski et al. 2010; Leung et al. 2019). The SEDs have been normalised at rest-frame 100 μm.

Compared to a typical SMG, Fig. 5 reveals that an extra $(2.8 \pm 0.9) \times 10^{11}$ $L_\odot$ emerges from HATLAS J084933-W across the rest-frame UV-optical wavelength regime, where it is a magnitude bluer in $g - K$. The SED of HATLAS J084933-W is, however, fully consistent with that of an SMG, lying at the upper boundary of the r.m.s. scatter in rest-frame UV–optical emission from typical SMGs, whereas we can see that an order of magnitude or more in flux density separates the SEDs of HATLAS J084933-W and the dusty Type-1 AGNs, across two orders of magnitude in wavelength, $\lambda_{\rm rest} \approx 0.15$–30 μm.

This illustrates the conundrum we face: the X-ray data for HATLAS J084933-W imply a colossal bolometric luminosity,[8] similar in magnitude to the far-IR luminosity, yet the latter arises from a large disk and cannot sensibly be powered by the AGN; unlike other dusty Type-1 AGN, there is no obvious sign of significant excess rest-frame UV–optical–mid-IR emission from the AGN, yet the accretion energy must be emerging somewhere, unless our understanding of how X-ray luminosity maps to bolometric luminosity is flawed. The panchromatic SED, low intrinsic X-ray absorption and general properties of HATLAS J084933-W therefore present a considerable puzzle.

[8] Determining the rest-frame 250 nm–2 keV slope using the observed optical magnitude would yield $\alpha_{\rm OX} \approx 1.1$, which would suggest a lower bolometric luminosity, yet this slope would then imply heavy UV obscuration; thus the approach taken in § 3 is physically meaningful and appropriate.

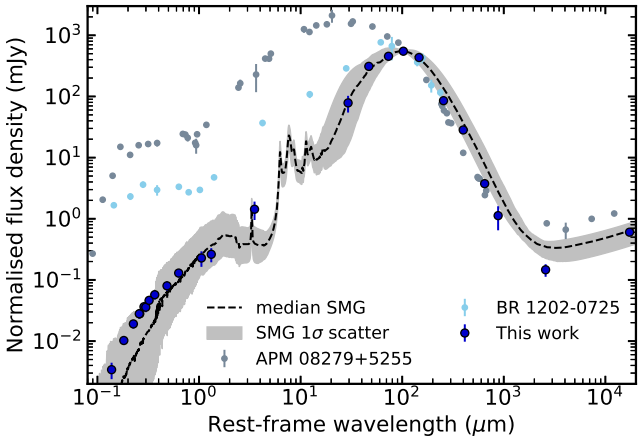

Figure 5. Rest-frame ultraviolet–through–radio SED of HATLAS J084933-W, with new photometry from the Hyper Suprime-Cam Subaru Strategic Program (Aihara et al. 2018) and from *WISE*. Also shown are the median SED of ALMA-identified SMGs [dashed line] in the Ultra-Deep Survey field (U. Dudzevičiūtė et al., in prep), where the grey area is the r.m.s. spread in SMG SEDs, and the SEDs of the Type-1 dust-rich quasars, APM 08279+5255, at $z = 3.9$ (Irwin et al. 1998; Leung et al. 2019) and BR 1202−0725, at $z = 4.7$ (McMahon et al. 1994; Leipski et al. 2010). The SEDs have been normalised at rest-frame 100 μm. Across rest-frame ≈ 0.15–30 μm, an order of magnitude or more in flux density separates the SEDs of HATLAS J084933-W and the dusty Type-1 AGNs.

A number of plausible scenarios could give rise to the observed configuration. We deal with three of them in what follows.

4.1 AGN seen through cavity in an unusually large disk?

Could a solution to the aforementioned conundrum be related to power of the AGN and the unusual extent of the dusty starburst in the galaxy hosting it? High-resolution spectroscopic imaging of component W of HATLAS J084933 has revealed molecular gas spread across a disk that is several times larger ($\approx$ 3–7 kpc FWHM, depending on the tracer) than the compact, $\approx$kpc submm continuum emission more typically found in SMGs (e.g. Ikarashi et al. 2015; Simpson et al. 2015; Oteo et al. 2017a,b; Hodge et al. 2019; Rujopakarn et al. 2019), irrespective of the presence in those SMGs of X-ray-detected AGN (Harrison et al. 2016). Such a powerful AGN will rapidly excavate a central cavity, perhaps with an ionisation cone oriented towards the NE that can go some way towards explaining the observed narrow-line properties,[9] perhaps leading to a relatively clear view of the broad-line region and little X-ray absorption along the line of sight through the disk[10] to a central AGN. It may also be possible that there is a contribution to the soft X-rays from photoionised gas and scattering within the ionisation cone, such that the true X-ray column is larger than that deduced from our simple model fit.

In this scenario, the observed extinction (see § 3) is due to gas and dust local to the AGN, i.e. its obscuring torus in the unified scheme, and/or along the line of sight through the host galaxy. $A_V \approx 2.2$ corresponds to over 7 mag of extinction at 125 nm, which is roughly the observed g band, such that we would see only the host galaxy in g, consistent with the observed properties and roughly 5 mag fainter than the prediction for the AGN before obscuration. We note that the apparent lack of hot dust emission is a problem for any model that invokes a conventional AGN torus.

If the X-ray opacity proves to be small compared to the dust attenuation implied by the Balmer decrement[11], this might indicate that the obscuration arises from a dusty, ionised outflow, akin to that identified by Mehdipour et al. (2012). Alternatively, if the AGN is obscured predominantly by dust in the surrounding galaxy then we would expect a a Seyfert-1-like [O III]/Hα ratio and a normal dust-to-gas ratio for the absorber, if we could combine measurements of X-ray absorption and the broad-line Balmer decrement. We could then calculate what fraction of the AGN power goes into heating the dust in the surrounding galaxy.

4.2 A second, unseen AGN?

In the absence of observations that tie down the broad-line Balmer decrement, or the spatial distribution of [O III]/Hβ, we can speculate that the absence of significant X-ray absorption — together with rest-frame optical features consistent with a Type-1 AGN — may imply that the accreting SMBH is not embedded in the gas-rich starburst. This would, in turn, suggest that energy due to accretion does not dominate the bolometric luminosity of HATLAS J084933-W.

I13 speculated that the mutual proximity and counter-rotation of the gas disks in components W and T might explain their unusual luminosities. Occam's razor might suggest instead that the near-naked SMBH we observe towards HATLAS J084933-W — modulo the lack of associated rest-frame UV–optical emission — is associated with another galaxy involved in a merger or interaction that triggered the starburst (e.g. Ellison et al. 2019).

HATLAS J084933-W would then be expected to contain a second SMBH, associated with the intense ongoing starburst, plausibly an unseen Compton-thick AGN. Sadly, although nearby binary AGN are occasionally revealed (e.g. in Mrk 739, at a distance of 130 Mpc, using *Chandra* – Koss et al. 2011), the observational challenges associated with demonstrating the presence of dual or binary AGN at even modest redshifts are similar or worse than those of identifying distant interactions and mergers, where the sensitivity and especially spatial resolution available to X-ray observers are rarely up to the task.

Largely because of SPIRE on the *Herschel Space Observatory* (Griffin et al. 2010; Pilbratt et al. 2010) and the wide-field ground-based imager, SCUBA-2 (Holland et al. 2013), many thousands of SMGs are now known (e.g. Eales et al. 2010; Oliver et al. 2012; Geach et al. 2017). While only a very small fraction of these rest-frame far-IR-selected galaxies are associated with Type-1 AGN, Knudsen et al. (2003) describe a submm-selected, intrinsically hyperluminous quasar, SMM J04135+10277, lensed by the galaxy cluster Abell 478, and *Herschel* led to the detection of many more (e.g. Ma & Yan 2015; Pitchford et al. 2016; Dong & Wu 2016). Some others have Type-2 AGN, or objects believed to be transitioning from Type-2 to Type-1 in the evolutionary scheme proposed by Sanders et al. (1988), e.g. the aforementioned SMM J02399−0136, with its BAL quasar. Follow-up submm detections of known optically-luminous quasars are relatively common (Isaak et al. 1994, 2002; Ivison 1995; Omont et al.

[9] The velocity offset between the narrow lines and the CO is then due to an outflow or winds towards the observer.

[10] I13 and Gómez et al. (2018) found disk inclinations of 56 ± 10° and $\approx$ 48° respectively, where 0° is face-on.

[11] Measuring the Balmer decrement will be relatively straightforward with H-band spectroscopy.

1996a; Priddey et al. 2003; Mainieri et al. 2005; Stacey et al. 2018; Hatziminaoglou et al. 2018, amongst others). The quasars BR 1202−0725 and BRI 1335−0417 were amongst the first to be detected at submm wavelengths, and were later found to have physically associated SMGs close by (Omont et al. 1996b; Yun et al. 2000; Carilli et al. 2002, 2013; Salomé et al. 2012; Wagg et al. 2012, 2014; Lu et al. 2017, see also Decarli et al. 2018, 2019; Venemans et al. 2018), one of which also harbours an X-ray-luminous AGN (Iono et al. 2006).

It is conceivable, then, that we have found a system that contains a HyLIRG, with a buried AGN, close to another more evolved quasar-like system. We cannot ignore the stark difference between the SED of HATLAS J084933-W and those of other quasars known to have SMG companions; however, a location in the outskirts or behind the gas-rich disk of HATLAS J084933-W may help explain why the Type-1 AGN is not bright at rest-frame UV–optical–mid-IR wavelengths. With sufficient separation, such a geometry might be revealed using the spatial resolution of *Chandra*, even if it could not be easily distinguished from our next suggestion.

4.3 An ejected AGN?

In another scenario — discussed in terms of a merging galaxy pair in the COSMOS field by Civano et al. (2012) — asymmetric emission of gravitational radiation (Peres 1962; Bekenstein 1973) during the coalescence of two SMBHs with anti-aligned spins (Campanelli et al. 2007; Lousto & Zlochower 2011a,b) and a high mass ratio (Baker et al. 2008) could have led to the ejection of the newly formed SMBH from the site of the merger, with a relative velocity as high as 5,000 km s^{-1}.

Such an ejected SMBH is thought unlikely to carry its narrow-line region along with it (Loeb 2007), but it could shine for 10^7 yr as a Type-1 AGN, and in an extremely gas-rich environment like that in HATLAS J084933-W — spanning several[12] kpc — the AGN would give rise to a narrow-line region as it travels.

We can further speculate that if the SMBH that we observe in X-rays and in the rest-frame optical has been ejected from the site of the merger, then the resulting lack of feedback via powerful AGN-driven winds (e.g. Maiolino et al. 2012; Veilleux et al. 2013, 2017; Cicone et al. 2014; Tombesi et al. 2015) — often invoked to regulate the growth of the stellar spheroidal component of the host galaxy and the SMBH itself (cf. Ramasawmy et al. 2019, cf. Grimmett et al. 2019) — may explain the extreme nature of the starburst in HATLAS J084933-W. Feedback from supernovae would be left as the primary regulation mechanism, perhaps enabling the object to skip quickly to the end of the aforementioned Sanders et al. sequence, from Compton-thick AGN to naked quasar. Indeed, recent theoretical work by McAlpine et al. (2019), based on cosmological hydrodynamical simulations, suggests that galaxies at $z \approx 2.5$ with high $L_{\rm IR}$ are able to reach and maintain large SFRs because their gas reservoirs are not depleted by accretion onto their central black holes, such that their black holes are under-massive. It would be interesting if — in HATLAS J084933-W — we have found an extreme example of this hypothesis, with the absence of a significantly massive black hole pushing its starburst firmly into the HyLIRG category.

Although undeniably interesting, the associated implication of this last scenario — that SMBHs may permeate intergalactic space — is not a topic for this paper.

[12] $\approx$ 7 kpc FWHM, as measured in CO J = 1–0 (I13) so $\approx 10^7$ yr at the maximum plausible velocity, or up to an order of magnitude higher at the measured line-of-sight velocity offset betweeen Hα + [N II] and CO.

5 SUMMARY AND CONCLUDING REMARKS

We report new X-ray, near-IR and submm observations of the starburst galaxies that comprise HATLAS J084933 at $z = 2.4$.

Our ALMA imaging confirms a more distant, fifth, dust- and gas-rich member, E, of the HATLAS J084933 protocluster, which is now known to cover $\approx$ 15 arcsec or $\approx$ 120 kpc. HATLAS J084933-E is extremely red, with an unusually broad CO J = 1–0 line; it may be a merger or a colossal disk.

Our *XMM-Newton* and KMOS imaging spectroscopy of HATLAS J084933-W — the brightest of the five galaxies, a HyLIRG, unlensed and extraordinarily luminous, even by the standards of SMGs — reveal the presence of an AGN. HATLAS J084933-W displays significant X-ray emission together with bright [N II] lines and a very broad Hα line; the latter implies $M_{\rm bh} \approx 2 \times 10^9$ M$_\odot$. For such a dusty and gas-rich host galaxy, we see surprisingly little intrinsic absorption towards the AGN, $N_{\rm H} \approx 5 \times 10^{21}$ cm^{-2}, likely with modest extinction, $A_V \approx 2$. Our estimate of the bolometric luminosity of the X-ray-bright AGN is commensurate with the far-IR luminosity of the starburst, yet we know from spatially resolved imaging spectroscopy that the system contains a colossal gas- and dust-rich disk, with no significant temperature gradient. Despite the AGN's potential to dominate the overall power budget, it is therefore not obvious that it does so.

We outline three plausible scenarios that could give rise to the observed characteristics of HATLAS J084933-W, though the lack of significant rest-frame UV–optical and/or mid-IR emission remains a puzzle in all of them.

Either we have a relatively clear view of the broad-line region through the starbursting disk of the host galaxy, with the powerful AGN having excavated a central cavity, or the AGN is not embedded in the starburst. In this second, prosaic option — where analogues are known — we speculate that there are two SMBHs: one, visible in X-rays, having evolved more quickly towards the naked quasar phase, in an unseen galaxy or galaxy remnant that lies very close to the HyLIRG; the second, buried deep within the dusty starburst, invisible to us.

In our third scenario, the observed SMBH has been ejected from the region experiencing the starburst, e.g. via asymmetric gravitational radiation during the coalescence of two SMBHs, and we postulate that the resulting absence of local AGN feedback may then explain the extreme nature of the starburst.

It is clear that there is considerably more to learn about the role and impact of the AGN or AGNs in HATLAS J084933. The intrinsic absorption is detected only barely and is poorly constrained, so it would be interesting to determine the degree of obscuration through which we are viewing the AGN. This could be achieved through a combination of deeper X-ray data — to more accurately measure the absorbing column and to determine whether it is dominated by reflection and/or has the strong 6.4-keV emission line that usually characterises this — and through rest-frame optical spectroscopy to measure the Balmer decrement of the broad emission lines. Mid-IR spectroscopy would also be useful to help disentangle the AGN/star formation contribution to the IR luminosity.

Our findings add to the growing body of evidence that powerful AGN are ubiquitous amongst HyLIRGs. However, the nature of the AGN observed in HATLAS J084933 is not at all what we expected and we cannot easily reconcile the high bolometric lu-

minosity and modest intrinsic absorption inferred from our X-ray observations with the large far-IR-emitting disk and the faint rest-frame UV–optical–mid-IR portion of its panchromatic SED.

ACKNOWLEDGEMENTS

We acknowledge the many contributions from Iván Oteo, the wisdom of Alain Omont and Ian Smail, and the generosity of Edith Falgarone, Hannah Stacey and Song Huang. We are also indebted to the anonymous referee for an excellent report.

RJI dedicates this paper to his long-time friend and colleague, Wayne Holland, who passed away in May 2019; without his immensely valuable contributions to submm instrumentation and astronomical research, we would still be waiting for ALMA.

This publication makes use of data products from the *Wide-field Infrared Survey Explorer*, which is a joint project of the University of California, Los Angeles, and the Jet Propulsion Laboratory/California Institute of Technology, funded by the National Aeronautics and Space Administration.

This paper makes use of the following ALMA data: ADS/JAO.ALMA#2013.1.00164.S. ALMA is a partnership of ESO (representing its member states), NSF (USA) and NINS (Japan), together with NRC (Canada), MOST and ASIAA (Taiwan), and KASI (Republic of Korea), in cooperation with the Republic of Chile. The Joint ALMA Observatory is operated by ESO, AUI/NRAO and NAOJ.

REFERENCES

Adelman-McCarthy J. K., et al., 2008, ApJS, 175, 297
Aihara H., et al., 2018, PASJ, 70, S8
Alexander D. M., Smail I., Bauer F. E., Chapman S. C., Blain A. W., Brandt W. N., Ivison R. J., 2005a, Nature, 434, 738
Alexander D. M., Bauer F. E., Chapman S. C., Smail I., Blain A. W., Brandt W. N., Ivison R. J., 2005b, ApJ, 632, 736
Baker J. G., Boggs W. D., Centrella J., Kelly B. J., McWilliams S. T., Miller M. C., van Meter J. R., 2008, ApJ, 682, L29
Bekenstein J. D., 1973, ApJ, 183, 657
Campanelli M., Lousto C., Zlochower Y., Merritt D., 2007, ApJ, 659, L5
Cardelli J. A., Clayton G. C., Mathis J. S., 1989, ApJ, 345, 245
Carilli C. L., et al., 2002, AJ, 123, 1838
Carilli C. L., Riechers D., Walter F., Maiolino R., Wagg J., Lentati L., McMahon R., Wolfe A., 2013, ApJ, 763, 120
Chabrier G., 2003, PASP, 115, 763
Cicone C., et al., 2014, A&A, 562, A21
Civano F., et al., 2012, ApJ, 752, 49
Cutri R. M., Huchra J. P., Low F. J., Brown R. L., Vanden Bout P. A., 1994, ApJ, 424, L65
Davies R. I., 2007, MNRAS, 375, 1099
Davies R. I., et al., 2013, A&A, 558, A56
Deane R. P., Rawlings S., Marshall P. J., Heywood I., Klöckner H.-R., Grainge K., Mauch T., Serjeant S., 2013, MNRAS, 430, 2
Decarli R., et al., 2018, ApJ, 854, 97
Decarli R., et al., 2019, arXiv e-prints, p. arXiv:1906.05308
Dong X. Y., Wu X.-B., 2016, ApJ, 824, 70
Eales S., et al., 2010, PASP, 122, 499
Efstathiou A., et al., 2014, MNRAS, 437, L16
Ellison S. L., Viswanathan A., Patton D. R., Bottrell C., McConnachie A. W., Gwyn S., Cuillandre J.-C., 2019, arXiv e-prints,
Elvis M., et al., 1994, ApJS, 95, 1
Falgarone E., et al., 2017, Nature, 548, 430
Franceschini A., Bassani L., Cappi M., Granato G. L., Malaguti G., Palazzi E., Persic M., 2000, A&A, 353, 910
Frayer D. T., Ivison R. J., Scoville N. Z., Yun M., Evans A. S., Smail I., Blain A. W., Kneib J., 1998, ApJ, 506, L7
Frayer D. T., Maddalena R. J., Ivison R. J., Smail I., Blain A. W., Vanden Bout P., 2018, ApJ, 860, 87
Freudling W., Romaniello M., Bramich D. M., Ballester P., Forchi V., García-Dabló C. E., Moehler S., Neeser M. J., 2013, A&A, 559, A96
Fu H., et al., 2013, Nature, 498, 338
Geach J. E., et al., 2017, MNRAS, 465, 1789
Gómez J. S., Messias H., Nagar N. M., Orellana G., Ivison R. J., van der Werf P., 2018, arXiv e-prints,
Graham J. R., Liu M. C., 1995, ApJ, 449, L29
Griffin M. J., et al., 2010, A&A, 518, L3+
Grimmett L. P., Mullaney J. R., Jin S., Bernhard E., Daddi E., Walters K., 2019, MNRAS, 487, 4071
Güver T., Özel F., 2009, MNRAS, 400, 2050
Harris A. I., et al., 2012, ApJ, 752, 152
Harrison C. M., et al., 2016, MNRAS, 457, L122
Hatziminaoglou E., Farrah D., Humphreys E., Manrique A., Pérez-Fournon I., Pitchford L. K., Salvador-Solé E., Wang L., 2018, MNRAS, 480, 4974
Hayward C. C., Kereš D., Jonsson P., Narayanan D., Cox T. J., Hernquist L., 2011, ApJ, 743, 159
Hines D. C., Wills B. J., 1993, ApJ, 415, 82
Hodge J. A., et al., 2019, ApJ, 876, 130
Holland W. S., et al., 2013, MNRAS, 430, 2513
Ikarashi S., et al., 2015, ApJ, 810, 133
Iono D., et al., 2006, ApJ, 645, L97
Irwin M. J., Ibata R. A., Lewis G. F., Totten E. J., 1998, ApJ, 505, 529
Isaak K. G., McMahon R. G., Hills R. E., Withington S., 1994, MNRAS, 269, L28
Isaak K. G., Priddey R. S., McMahon R. G., Omont A., Peroux C., Sharp R. G., Withington S., 2002, MNRAS, 329, 149
Ivison R. J., 1995, MNRAS, 275, L33
Ivison R. J., Smail I., Le Borgne J., Blain A. W., Kneib J., Bezecourt J., Kerr T. H., Davies J. K., 1998, MNRAS, 298, 583
Ivison R. J., et al., 2004, ApJS, 154, 124
Ivison R. J., Smail I., Papadopoulos P. P., Wold I., Richard J., Swinbank A. M., Kneib J.-P., Owen F. N., 2010, MNRAS, 404, 198
Ivison R. J., et al., 2013, ApJ, 772, 137
Just D. W., Brandt W. N., Shemmer O., Steffen A. T., Schneider D. P., Chartas G., Garmire G. P., 2007, ApJ, 665, 1004
Karim A., et al., 2013, MNRAS, 432, 2
Kennicutt Jr. R. C., 1998, ApJ, 498, 541
Knudsen K. K., van der Werf P. P., Jaffe W., 2003, A&A, 411, 343
Kocevski D. D., et al., 2018, ApJS, 236, 48
Koss M., et al., 2011, ApJ, 735, L42
Lacy M., et al., 2004, ApJS, 154, 166
Leipski C., et al., 2010, A&A, 518, L34
Leung T. K. D., Hayward C. C., Casey C. M., Staguhn J., Kovacs A., Dowell C. D., 2019, ApJ, 876, 48
Litke K. C., et al., 2019, ApJ, 870, 80
Loaring N. S., et al., 2005, MNRAS, 362, 1371
Loeb A., 2007, Physical Review Letters, 99, 041103
Lousto C. O., Zlochower Y., 2011a, Phys. Rev. D, 83, 024003
Lousto C. O., Zlochower Y., 2011b, Physical Review Letters, 107, 231102
Lu N., et al., 2017, ApJ, 842, L16
Lumb D. H., Warwick R. S., Page M., De Luca A., 2002, A&A, 389, 93
Lusso E., et al., 2012, MNRAS, 425, 623
Lutz D., Tacconi L. J., 1999, Ap&SS, 266
Ma Z., Yan H., 2015, ApJ, 811, 58
Mainieri V., et al., 2005, MNRAS, 356, 1571
Maiolino R., et al., 2012, MNRAS, 425, L66
Mateos S., et al., 2005, A&A, 433, 855
Mateos S., et al., 2010, A&A, 510, A35
McAlpine S., et al., 2019, MNRAS, p. 1605
McMahon R. G., Omont A., Bergeron J., Kreysa E., Haslam C. G. T., 1994, MNRAS, 267, L9

McMullin J. P., Waters B., Schiebel D., Young W., Golap K., 2007, in Shaw R. A., Hill F., Bell D. J., eds, Astronomical Society of the Pacific Conference Series Vol. 376, Astronomical Data Analysis Software and Systems XVI. p. 127
Mehdipour M., Branduardi-Raymont G., Page M. J., 2012, A&A, 542, A30
Menéndez-Delmestre K., Blain A. W., Swinbank M., Smail I., Ivison R. J., Chapman S. C., Gonçalves T. S., 2013, ApJ, 767, 151
Narayanan D., et al., 2015, Nature, 525, 496
Oliver S. J., et al., 2012, MNRAS, 424, 1614
Omont A., McMahon R. G., Cox P., Kreysa E., Bergeron J., Pajot F., Storrie-Lombardi L. J., 1996a, A&A, 315, 1
Omont A., Petitjean P., Guilloteau S., McMahon R. G., Solomon P. M., Pécontal E., 1996b, Nature, 382, 428
Oteo I., et al., 2016, ApJ, 827, 34
Oteo I., et al., 2017a, preprint, (arXiv:1709.04191)
Oteo I., Zwaan M. A., Ivison R. J., Smail I., Biggs A. D., 2017b, ApJ, 837, 182
Oteo I., et al., 2018, ApJ, 856, 72
Page M. J., Davis S. W., Salvi N. J., 2003, MNRAS, 343, 1241
Panessa F., Bassani L., Cappi M., Dadina M., Barcons X., Carrera F. J., Ho L. C., Iwasawa K., 2006, A&A, 455, 173
Peres A., 1962, Phys. Rev., 128, 2471
Pilbratt G. L., et al., 2010, A&A, 518, L1+
Pitchford L. K., et al., 2016, MNRAS, 462, 4067
Priddey R. S., Isaak K. G., McMahon R. G., Omont A., 2003, MNRAS, 339, 1183
Ramasawmy J., Stevens J., Martin G., Geach J. E., 2019, MNRAS, 486, 4320
Richards G. T., et al., 2006, ApJS, 166, 470
Riechers D. A., et al., 2013, Nature, 496, 329
Riechers D. A., et al., 2017, ApJ, 850, 1
Rosen S. R., et al., 2016, A&A, 590, A1
Rowan-Robinson M., Wang L., 2010, MNRAS, 406, 720
Rowan-Robinson M., et al., 1991, Nature, 351, 719
Ruiz A., Carrera F. J., Panessa F., 2007, A&A, 471, 775
Rujopakarn W., et al., 2019, arXiv e-prints, p. arXiv:1904.04507
Salomé P., Guélin M., Downes D., Cox P., Guilloteau S., Omont A., Gavazzi R., Neri R., 2012, A&A, 545, A57
Sanders D. B., Soifer B. T., Elias J. H., Madore B. F., Matthews K., Neugebauer G., Scoville N. Z., 1988, ApJ, 325, 74
Schulze A., et al., 2018, ApJS, 239, 22
Simpson J. M., et al., 2015, ApJ, 799, 81
Simpson J. M., et al., 2017, ApJ, 839, 58
Stacey H. R., et al., 2018, MNRAS, 476, 5075
Stach S. M., et al., 2019, MNRAS, 487, 4648
Strateva I. V., Brandt W. N., Schneider D. P., Vanden Berk D. G., Vignali C., 2005, AJ, 130, 387
Tombesi F., Meléndez M., Veilleux S., Reeves J. N., González-Alfonso E., Reynolds C. S., 2015, Nature, 519, 436
Valiante E., et al., 2016, MNRAS, 462, 3146
Veilleux S., et al., 2013, ApJ, 776, 27
Veilleux S., Bolatto A., Tombesi F., Meléndez M., Sturm E., González-Alfonso E., Fischer J., Rupke D. S. N., 2017, ApJ, 843, 18
Venemans B. P., et al., 2018, ApJ, 866, 159
Vernet J., Cimatti A., 2001, A&A, 380, 409
Wagg J., et al., 2012, ApJ, 752, L30
Wagg J., et al., 2014, ApJ, 783, 71
Wright E. L., et al., 2010, AJ, 140, 1868
Younger J. D., et al., 2007, ApJ, 671, 1531
Younger J. D., et al., 2008, ApJ, 688, 59
Yun M. S., Carilli C. L., Kawabe R., Tutui Y., Kohno K., Ohta K., 2000, ApJ, 528, 171
Zhang Z.-Y., Romano D., Ivison R. J., Papadopoulos P. P., Matteucci F., 2018, Nature, 558, 260